Bound exciton luminescence in shock compressed GaP:S and GaP:N

P. Grivickas,[1,a)] M. D. McCluskey,[1] Y. M. Gupta,[1] Y. Zhang,[2] and J. F. Geisz[2]
[1]*Department of Physics and Astronomy and Institute for Shock Physics, Washington State University, Pullman, Washington 99164-2816, USA*
[2]*National Renewable Energy Laboratory, 1617 Cole Blvd., Golden, Colorado 80401, USA*

(Received 26 September 2008; accepted 3 June 2009; published online 22 July 2009)

Photoluminescence (PL) spectra of bound excitons were measured in uniaxially strained GaP by performing shock-wave experiments at liquid nitrogen temperatures. GaP samples doped with sulfur or nitrogen were compressed up to 3 GPa when subjected to uniaxial strains along the [100] crystallographic orientation. PL lines from shallow sulfur donors redshifted upon compression, tracking the reduction in the indirect band gap. PL lines related to the isoelectronic NN_1 pairs, in contrast, exhibited splitting and nonlinear blueshift. An empirical approach was used to model the NN_1 behavior. It was shown that the splitting pattern is consistent with the previously proposed symmetry of NN_1 defects and nonlinearities resulting from the reduction in the exciton binding energy. At high stresses, the NN_1 lines disappeared due to the ionization of bound excitons. © *2009 American Institute of Physics*. [DOI: 10.1063/1.3159641]

I. INTRODUCTION

Applications such as multijunction solar cells fueled a resurgence in dilute nitride semiconductor research.[1] Isoelectronic nitrogen impurities in GaP have been studied extensively for over 40 years. Thomas *et al.*[2,3] showed that the incorporation of isoelectronic nitrogen in GaP leads to the emergence of an impurity state in the band gap, which acts as an efficient trap for free excitons. With increasing nitrogen concentration, a series of deep traps appear due to nitrogen atoms located at neighboring lattice sites, the so-called NN pairs. Recent advances in material growth technologies pushed nitrogen concentrations to several percent. These alloys contain even deeper band gap states, attributed to nitrogen clusters.[4]

In contrast with the well-established behavior of shallow donors and acceptors in III–V semiconductors,[5] the formation of electronic states due to the isoelectronic nitrogen dopants and clusters is quite complicated. Several theories were proposed to elucidate experimental results including impurity band formation,[4] polymorphous alloy,[6] and the band anticrossing[7,8] models. The behavior of nitrogen in GaP, especially in the alloying regime, still generates considerable scientific debate.[9–12]

Experiments involving applied stress played an important role in evaluating theoretical predictions for GaP:N. Application of hydrostatic pressure to low-doped samples[13] revealed nonlinear pressure dependences of exciton binding energies at the NN traps. Extension of these measurements to 10 GPa[14,15] showed that the pressure-induced reduction in exciton binding energy causes the PL peaks to disappear and so-called *ionization pressures* were determined for all NN peaks. Similar nonmonotonic pressure behavior was also observed in heavily doped alloys.[7,15] At high hydrostatic pressures achieved in alloys, changes in pressure dependences were interpreted as anticrossing between the localized nitrogen states and the *X* conduction minima of the host GaP.[8]

Uniaxial stress experiments probe individual electronic levels by reducing the symmetry of the defects. At dilute nitrogen concentrations, the splitting of PL lines allowed researchers to analyze the *j-j* coupling scheme for excitons bound to single nitrogen atoms.[16,17] In higher doped samples, the splitting pattern was analyzed to deduce the local symmetry of the NN pairs[18] and the NN_2 triplet.[19] Uniaxial stress measurements, however, are limited to stresses well below 1 GPa due to the elastic limit of single crystals. These stresses are far below the *ionization stresses* that are required to bring deep NN states[20] into resonance with the conduction band edge.

Plane shock-wave experiments lower the crystal symmetry due to uniaxial strain along the direction of wave propagation. Unlike uniaxial stress loading, shock compression can produce longitudinal stresses up to 10 GPa in semiconductors.[21,22] Because the uniaxial strain state is a transient state, data must be obtained within several hundreds of nanoseconds. Recently, shock compression experiments combined with optical measurements were used to investigate band-gap transitions in uniaxially strained GaP (Ref. 23) and to obtain an accurate set of deformation potentials for this semiconductor.[24]

In the present work, we measured the PL spectra of sulfur and nitrogen bound excitons in GaP samples shock compressed along the [100] crystallographic axis. Due to the large longitudinal stresses achieved in our experiments, we were able to observe the nonlinear shifts of NN_1 peaks up to their intersection with the *X* conduction band. Combining these results with previous data from hydrostatic pressure and uniaxial stress experiments, we obtained a complete model for NN_1 pairs in strained GaP.

II. EXPERIMENTS

The experimental configuration for photoluminescence (PL) measurements in shock-wave experiments is shown

a)Electronic mail: pgrivickas@wsu.edu.

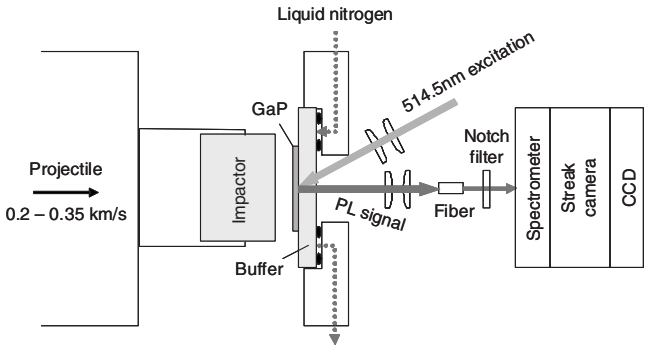

FIG. 1. Diagram of PL measurements in shock-wave experiments.

schematically in Fig. 1. 10×10 mm^2 samples were cut from [100] oriented GaP wafers. Sulfur-containing wafers were uniformly doped across the 400 μm thickness to a concentration of $1-3\times10^{18}$ cm^{-3}. Nitrogen-containing $GaP_{1-x}N_x$ epilayers were grown by metal organic chemical vapor deposition on 320 μm thick Zn-doped substrates to a thickness of 3 μm using triethylgallium, phosphine, and dimethylhydrazine sources at 700 °C.[25] The nitrogen composition was determined to be $x=0.07\%$ from high resolution x-ray diffraction measurements, corresponding to a nitrogen concentration of 1.7×10^{19} cm^{-3}.

Samples were bonded to *c*-cut sapphire buffer windows using optically transparent epoxy (<2 μm thickness bond). Nitrogen-containing samples had epilayers facing the sapphire buffer. The sample assembly was mechanically attached to an aluminum holder and cooled using liquid nitrogen. Shock waves in each sample were produced by impacting the front surface of the GaP samples with an impactor (*z*-cut quartz or poly(methyl methacrylate) (PMMA)) mounted on a projectile and accelerated to the desired velocity using a gas gun. After the impact, shock waves were propagating across the sample creating different longitudinal stress states at the probed GaP-buffer interface as illustrated by the *t*-*x* diagram in Fig. 2(a), where *x* is the impact direction. Due to the impedance mismatch between the sample and the impactor/buffer materials, the probed GaP surface underwent the stress states *A* and *B* until reaching the steady state *C*. The latter state persisted until the arrival of release waves from the free surface of the buffer, resulting in the states *D* and *E*. The experiment was terminated when edge waves arrived from the lateral sample edges.

TABLE I. Longitudinal stresses (GPa) achieved in the different states of the three experimental configurations.

	Experiment		
State	(a) Quartz→GaP-sapphire; 224 m/s	(b) PMMA→GaP-sapphire; 475 m/s	(c) PMMA→GaP-sapphire; 288 m/s
A	2.94	2.11	1.24
B	2.8	1.65	0.96
C	2.81	1.7	1
D	0.72	0.21	0.12
E	1.75	1.27	1.08

Longitudinal stress (σ) values in each state depended on the impactor material and its velocity. Three different experimental configurations, used in this work, are shown in Table I. Exact longitudinal stress-time profiles calculated[26] for the three cases are shown in Fig. 2(b). Longitudinal stresses corresponding to each of the five states are summarized in Table I. From the well-established shock response of *c*-cut sapphire,[27] *z*-cut quartz,[28] and PMMA,[29] the stress values in state *C* are accurate to within 1%. Stress values in the reverberation states *A* and *B* and the release states *D* and *E* were calculated using a linear elastic response of the GaP along the [100] orientation.[30] Comparison between the calculated and measured particle velocities for GaP at 6 GPa showed that the total error is below 3%.

Changes in optical spectra at different longitudinal stresses were observed using time-resolved PL measurements. During the compression, the center of the probed sample surface was excited by a single 1.5 μs duration pulse from a dye laser operating at 514.5 nm wavelength. The long duration of the excitation pulse allowed a continuous collection of optical signal with the arrival of new shock states. The PL emission was collected from a 400 μm probe spot within the excited area, focused into an optical fiber, spectrally dispersed by an imaging dual-grating spectrometer,

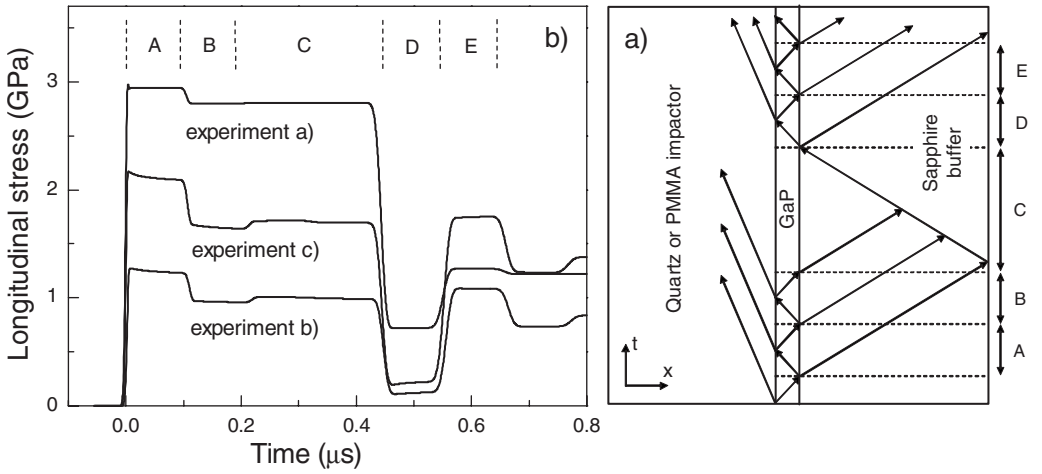

FIG. 2. Evolution of longitudinal stress in shock experiments. (a) Time dependence at the probed sample-window interface for the three different experimental configurations. (b) Wave propagation paths in the impactor-target system after the impact.

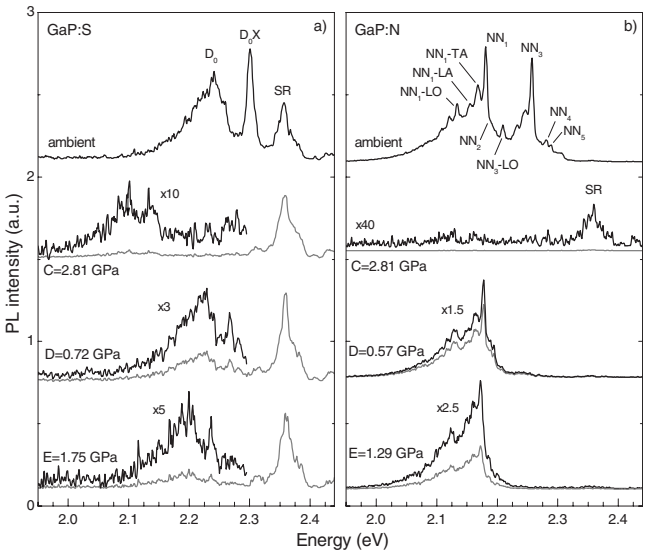

FIG. 3. PL of (a) GaP:S and (b) GaP:N samples in the different longitudinal stress states of the (a) experimental configuration.

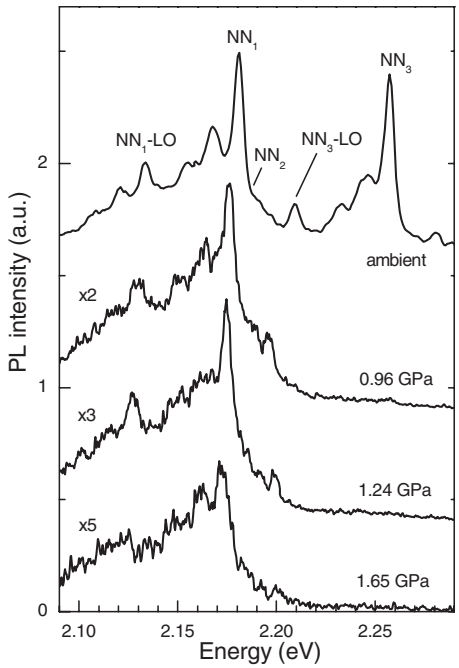

FIG. 4. Changes in the PL around the NN_1 peak with increasing longitudinal stress.

temporally dispersed by an electronic streak camera, and digitally recorded on a two-dimensional charge-coupled device array. Final data sets consisted of three dimensional plots showing PL intensity versus wavelength and time. The ~25 ns time resolution of the system was sufficient to assign PL spectra to individual >100 ns long shock states [Fig. 2(b)]. Details regarding the optical measurements in single event compression experiments can be found elsewhere.[23,31,32]

III. RESULTS

A. PL spectra

Ambient PL spectra of GaP:S and GaP:N samples at liquid nitrogen temperature are shown in the top part of Figs. 3(a) and 3(b), respectively. Recombination of excitons bound to neutral sulfur donors in GaP:S results in a single narrow D_0X peak at 2.301 eV.[33] At lower energies, this peak is accompanied by a much broader D_0 peak originating from the recombination of free holes at neutral sulfur donors.[34] At higher energies, the sapphire Raman lines (labeled SR) generated in the sapphire buffer window were also observed. The spectrum of GaP:N consists of several NN_i emission lines and their pronounced phonon replicas in the 2.1–2.3 eV energy range. These NN_i lines originate from the recombination of an exciton bound to a pair of nitrogen atoms with different separations or orientations.[35] Raman lines from the sapphire buffer windows were almost negligible in the GaP:N spectrum due to the low excitation energies required for efficient PL.

Figure 3(a) shows the PL spectra of GaP:S collected in the *C*, *D*, and *E* states of the (a) experimental configuration in Fig. 2(b). Despite the decreasing signal intensity, distinct D_0X peaks were identified in each state and showed a stress-dependent redshift. This behavior was previously observed for GaP:S shocked along the [100], [111], and [110] orientations.[24] It was shown that sulfur bound excitons correspond to near band-edge transitions resulting from the split and shift of electronic states in GaP under uniaxial strain.[23]

Figure 3(b) shows PL spectra of GaP:N in the same states of the (a) experimental configuration. In the high-stress *C* state (as well as the preceding states *A* and *B*, not shown), all NN_i pair related peaks disappeared from the spectrum, and only the weak SR lines were observed. Similar behavior has been observed in the hydrostatic pressure experiments and attributed to the "pressure ionization" of NN_i bound excitons.[15]

In the *D* and *E* release states, the PL spectrum around the lowest energy NN_1 pair was recovered. NN_i pairs with $i>1$ were not observed at the applied longitudinal stresses. The strongest peak in the recovered spectrum and its accompanying structure on the low energy side had clear similarities to the ambient NN_1 line and its phonon replicas, but were slightly redshifted. The high energy side of the strongest peak revealed several weak but distinct peaks absent in the ambient spectrum. These revealed peaks were measured using higher spectral resolution, as shown in Fig. 4.

The shift of the NN_1 line and the revealed peaks are shown by the symbols in Fig. 5. The shift of the *X* conduction band, determined from the D_0X peak for GaP:S under [100] uniaxial strain, is also shown. With increasing longitudinal stresses, the NN_1 line and the revealed peaks approach the downwards moving *X* conduction band, suggesting their eventual merger. The evolving NN_1 peak pattern also resembles a split of a degenerate energy state and is analyzed in detail in the next section.

B. PL intensity

In shock experiments, the PL signal from the same sample position is continuously recorded as it experiences different longitudinal stress states. Such data allow a direct

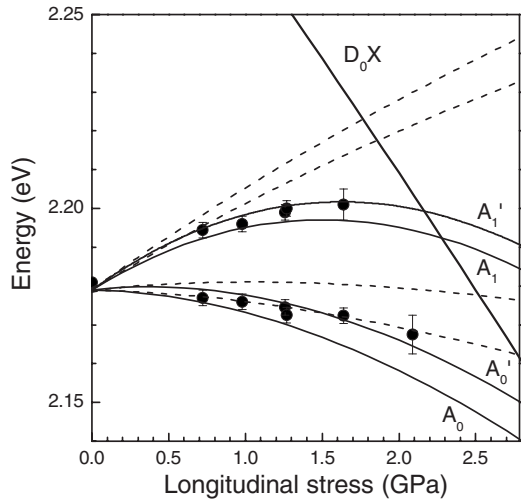

FIG. 5. Shift and splitting of the NN_1 related peaks (data points) with respect to the downwards moving D_0X peak (solid line) at increasing longitudinal stresses. Lines show theoretical data modeling using linear (dashed lines) and quadratic correction (solid lines) approximations.

comparison of PL intensities at ambient and shocked conditions. At ambient conditions, the integrated PL intensity from the D_0X and D_0 peaks in GaP:S followed the temporal profile of the dye laser pulse intensity. During shock experiments, the PL signal initially followed the laser pulse and then decreased abruptly upon impact. The evolution of the PL intensity in shocked GaP:S, normalized to the ambient signal, is shown in Fig. 6(a) by the solid line. The data correlate well with the longitudinal stress profile at the probed surface (dashed line).

At ambient conditions, the integrated PL intensity of the NN_1 peak and its phonon replicas in GaP:N had a clear saturation level in comparison to the temporal profile of the dye laser pulse, indicating a finite concentration of NN_1 traps. During shock experiments, the PL signal also followed the evolution of longitudinal stress, as shown by the normalized PL intensities in Fig. 6(b).

Normalized PL intensities for different shocked states of GaP:S and GaP:N samples are plotted in Fig. 7 by the open and solid symbols, respectively. GaP:S results at stresses higher than 2.8 GPa were obtained in experiments described in Ref. 24. In GaP:S, the PL intensities show an initial discontinuous decrease at low longitudinal stresses, followed by an exponential decay (dashed line in Fig. 7). Similar behavior was observed in the optical absorption strength of the lowest band-to-band absorption edge of shocked GaP:S.[23] The loss of PL intensity, therefore, may be due to a reduction in the conduction-band density of states that occurs when the X-band is split.

In GaP:N, no discontinuous changes were observed at low strains, reflecting the differences between the wave functions of shallow S donors and highly localized NN centers. Wave functions of localized impurities spread throughout the whole Brillouin zone and are insensitive to the changes in the density of states at a particular k-point.[15] At longitudinal stresses <2 GPa, luminescence related to NN_1 pairs showed an exponential decrease with increasing longitudinal stress.

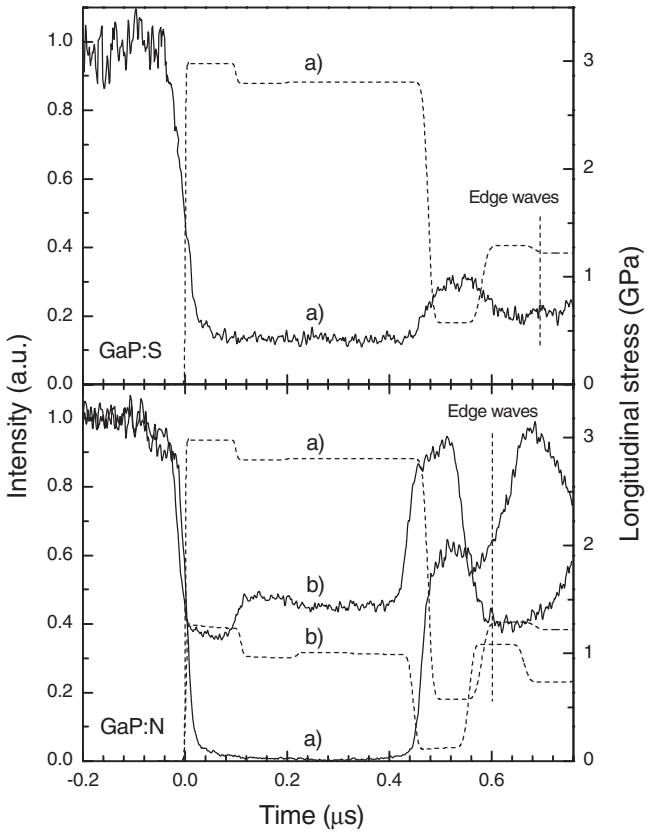

FIG. 6. Evolution of the normalized integrated PL intensity from the D_0X and D_0 peaks in GaP:S (upper figure) and the NN_1 peak and its phonon replicas in GaP:N (lower figure) in different experimental configurations. Dashed lines show the corresponding time dependence of the longitudinal stress.

At longitudinal stresses ~ 2 GPa, the NN_1 peak related intensity decreased abruptly, consistent with ionization of the bound excitons.

IV. ANALYSIS AND DISCUSSION

A. Energy levels

The NN_1 line originates from recombination of excitons bound to the NN pairs oriented along the $[aa0]$ or equivalent

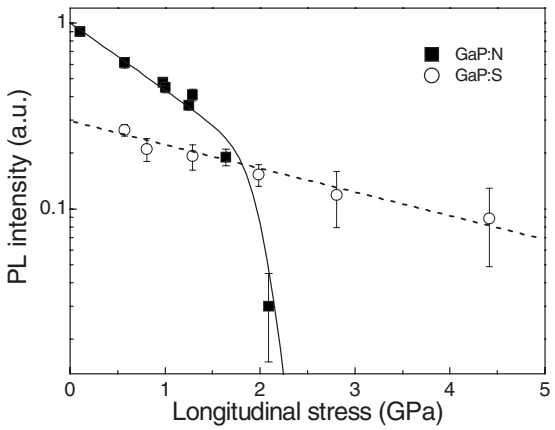

FIG. 7. Normalized integrated PL intensity from the D_0X and D_0 peaks in GaP:S (open symbols) and the NN_1 peak and its phonon replicas in GaP:N (solid symbols) vs longitudinal stresses. Lines show theoretical data modeling.

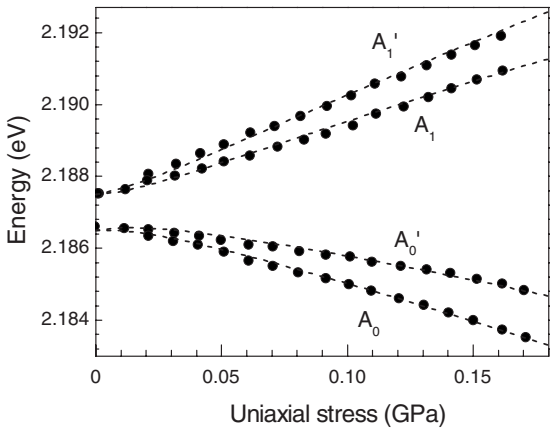

FIG. 8. Shift and splitting of the NN_1 peak (data points) under the uniaxial stresses applied along the [100] crystallographic axis of GaP (from Ref. 18). Dashed lines show theoretical data modeling.

crystal directions.[18] At liquid nitrogen temperatures, only transitions from the dipole-allowed states A in the j-j coupling scheme retain their optical strength.[36] Deformation along the [100] direction lifts the degeneracy of the A manifold in two ways. First, the wave function of the hole in the bound exciton follows the splitting of the $|\frac{1}{2}\rangle$ and $|\frac{3}{2}\rangle$ valence bands, resulting in the two components A_0 and A_1. Second, the wave function of the electron experiences different axial deformations near the differently oriented NN_1 pairs, splitting each component into unprimed and primed subcomponents: A_0, A_1 and A_0', A_1'. To first order, the reduction in binding energy E_B=124 meV (Ref. 20) of NN_1 bound excitons is proportional to the shear e_1-e_2 and hydrostatic e_1+2e_2 contributions of the applied deformation:

$$E_{A_0} = E_X - E_B[1 + B_1(e_1 - e_2) + C(e_1 + 2e_2)],$$

$$E_{A_1} = E_X - E_B[1 + B_2(e_1 - e_2) + C(e_1 + 2e_2)],$$

$$E_{A_0'} = E_X - E_B[1 + B_3(e_1 - e_2) + C(e_1 + 2e_2)],$$

$$E_{A_1'} = E_X - E_B[1 + B_4(e_1 - e_2) + C(e_1 + 2e_2)], \quad (1)$$

where e_1 and e_2 are the strains parallel and perpendicular to the [100] direction, respectively; E_X is the X conduction band minimum; the B and C coefficients are empirical deformation potentials. At ambient conditions, the local strain field surrounding the NN_1 pairs is sufficient to split the hole wave functions, resulting into two energy peaks.[36] This small perturbation can be modeled by introducing the j-j coupling parameter Δ_0=0.5 meV,

$$E = \tfrac{1}{2}[E_{A_0} + E_{A_1} \pm \sqrt{[E_{A_0} - E_{A_1}]^2 + 4\Delta_0^2}],$$

$$E' = \tfrac{1}{2}[E_{A_0'} + E_{A_1'} \pm \sqrt{[E_{A_0'} - E_{A_1'}]^2 + 4\Delta_0^2}]. \quad (2)$$

B. Uniaxial stress

For uniaxial stress σ applied along the [100] direction, the strain components are given by

TABLE II. Empirical deformation potentials used in modeling the NN_1 peak shifts under different deformations in GaP:N.

Deformation potential	Value
B_1	−36
B_2	−60
B_3	−31
B_4	−56
C	−20
D_1	0.25
D_2	0.15

$$e_1 = \frac{C_{11} + C_{12}}{(C_{11} - C_{12})(C_{11} + 2C_{12})}|\sigma| \quad \text{and} \quad e_2 = -\frac{C_{12}}{C_{11} + C_{12}} e_1. \quad (3)$$

We consider that positive e values correspond to compressive strain. The elastic constants of GaP are C_{11}=141.2 GPa and C_{12}=62.5 GPa.[30] In the considered uniaxial stress range, the reported shift in E_X versus [100] stress is approximately −0.09 eV/GPa.[37] The uniaxial stress data of Ref. 18 were modeled using Eq. (1)–(3). The results are shown by the dashed lines in Fig. 8. The coefficients B and C used for fitting the data are summarized in Table II.

C. Hydrostatic pressure

For hydrostatic pressure P, the strain is given by

$$e_1 = e_2 = P/(C_{11} + 2C_{12}). \quad (4)$$

This reduces Eq. (1) to a single first-order shift,

$$E = E_X - E_B[1 + 3Ce_1], \quad (5)$$

where the reported shift of E_X versus pressure is −0.015 eV/GPa.[15] The prediction from Eq. (5), using the determined coefficient C (Table II), is shown by the dashed line in Fig. 9. The PL energies obtained in Ref. 15 agree with the prediction at low pressures, but exhibit a diverging nonlinear shift at high pressures (symbols in Fig. 9). It was shown that such nonlinearity can be qualitatively understood by a simple

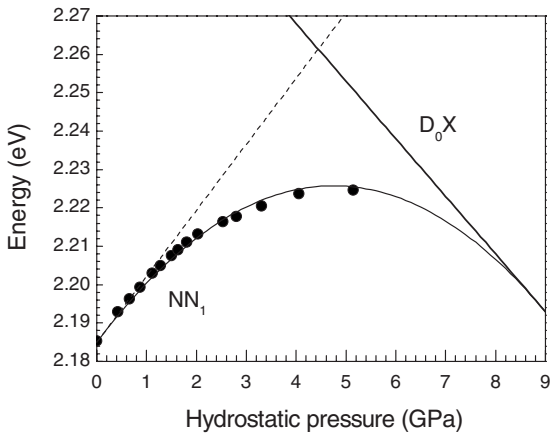

FIG. 9. Shift of the NN_1 peak (data points) under the hydrostatic pressure (from Ref. 15). Lines show theoretical data modeling using linear (dashed line) and quadratic correction (solid line) approximations.

square-well potential model in the limit of a short-range interaction.[13] The model introduces a term that is proportional to the square of the linear shift. The addition of this term to Eq. (5) yields

$$E = E_X - E_B[1 + 3Ce_1] - D_1E_B[3Ce_1]^2. \quad (6)$$

A good data fit by Eq. (6) is shown by the solid line in Fig. 9. The fitting coefficient D_1 for the nonlinear behavior is listed in Table II. The observation that the solid line in Fig. 9 is tangential to the X-band minimum is consistent with the square-well potential model.

D. Shock compression

Our shock compression experiments resulted in uniaxial strain given by

$$e_1 = |\sigma|/C_{11} \quad \text{and} \quad e_2 = 0. \quad (7)$$

Using Eq. (1), the obtained deformation potentials B and C (Table II) and the determined E_X versus longitudinal stress dependence of -0.06 eV/GPa,[24] we get the result shown by the dashed lines in Fig. 5. The limited resolution of our experiments did not allow us to observe the orientational splitting of the A_0 and A_1 lines into their primed subcomponents. With increasing longitudinal stress the experimental PL energies diverge from the predicted linear shift. As in the case of hydrostatic pressure, we introduced a quadratic correction term to account for this nonlinearity,

$$E_{A_0} = E_X - E_B[1 + (B_1 + C)e_1] - D_2E_B[(B_1 + C)e_1]^2,$$

$$E_{A_1} = E_X - E_B[1 + (B_2 + C)e_1] - D_2E_B[(B_2 + C)e_1]^2,$$

$$E_{A_0'} = E_X - E_B[1 + (B_3 + C)e_1] - D_2E_B[(B_3 + C)e_1]^2,$$

$$E_{A_1'} = E_X - E_B[1 + (B_4 + C)e_1] - D_2E_B[(B_4 + C)e_1]^2. \quad (8)$$

The best data fit using Eq. (8) yields the solid lines in Fig. 5. The fitting coefficient D_2 is provided in Table II. The relatively weak quadratic correction term ($D_2 < D_1$) indicates that a simple square-well potential model ceases to be a good approximation for the bound exciton interactions under uniaxial strain.

The ionization of bound excitons was confirmed using the PL intensity measurements. It was shown previously[33] that the reduction in PL intensity due to the thermal ionization can be expressed as

$$I(T) = I_0/[1 + K\exp(-E_T/kT)], \quad (9)$$

$$E_T = E_B + E_{\text{ex}}, \quad (10)$$

where I_0 is the PL intensity in the limit $T \to 0$ K, K is a temperature independent constant, and k is Boltzmann's constant. E_T is the thermal ionization energy, where $E_{\text{ex}} = -22$ meV (Ref. 20) is the binding energy of free excitons. We assume that a similar expression is valid for uniaxially strained GaP,

$$I(e_1) = I_0\exp(-e_1/e_C)/[1 + K\exp(-E_T(e_1)/kT)], \quad (11)$$

$$E_T(e_1) = E_B + E_{\text{ex}} - \Delta E_X(e_1) - \Delta E_B(e_1), \quad (12)$$

where the $\exp(-e_1/e_C)$ term is introduced to account for the exponential PL decrease due to strain; $\Delta E_X(e_1)$ and $\Delta E_B(e_1)$ represent the reduction in the thermal ionization energy due to the uniaxial strain as described by Eq. (8). Equation (11) was normalized to zero-stress intensity [Eq. (9)] and used to fit the experimental data. A good fit was obtained using $e_C = 0.85\%$ and $K = 150$, as shown by the solid line in Fig. 7. This result shows that the ionization of bound excitons is responsible for the disappearance of the NN_1 peaks in the spectra of GaP:N at high longitudinal stresses.

V. CONCLUSIONS

We observed changes in the PL spectra of excitons bound to shallow sulfur donors and isoelectronic NN pairs under shock wave uniaxial compression. The sulfur bound excitons shifted to lower energies upon compression, tracking the changes of the indirect band gap of GaP. The NN bound excitons showed splitting and nonlinear shifts. The observed splitting pattern of the NN_1 pair was consistent with the previously proposed symmetry of this defect. The nonlinear shifts of NN_1 bound excitons were weaker than predicted by a simple square-well potential model and resulted in the ionization of bound excitons due to the downward shift of the X conduction band. These observations point to the fundamental differences in the attractive potential near the shallow sulfur donors and the strongly localized NN pairs.

ACKNOWLEDGMENTS

The authors thank K. Zimmerman and K. Perkins for their help in performing the experiments. This work was supported by DOE Grant DE-FG03-97SF21388. M.D.M. acknowledges partial support from NSF.

[1] I. Vurgaftman and J. R. Meyer, J. Appl. Phys. **94**, 3675 (2003).
[2] D. G. Thomas, J. J. Hopfield, and C. J. Frosch, Phys. Rev. Lett. **15**, 857 (1965).
[3] D. G. Thomas and J. J. Hopfield, Phys. Rev. **150**, 680 (1966).
[4] Y. Zhang, B. Fluegel, A. Mascarenhas, H. P. Xin, and C. W. Tu, Phys. Rev. B **62**, 4493 (2000).
[5] E. F. Schubert, *Doping in III-V Semiconductors* (Cambridge University Press, Cambridge, 1993).
[6] P. R. C. Kent and A. Zunger, Phys. Rev. B **64**, 115208 (2001).
[7] W. Shan, W. Walukiewicz, K. M. Yu, J. Wu, J. W. Ager III, E. E. Haller, H. P. Xin, and C. W. Tu, Appl. Phys. Lett. **76**, 3251 (2000).
[8] J. Wu, W. Walukiewicz, K. M. Yu, J. W. Ager III, E. E. Haller, Y. G. Hong, H. P. Xin, and C. W. Tu, Phys. Rev. B **65**, 241303(R) (2002).
[9] I. A. Buyanova, M. Izadifard, A. Kasic, H. Arwin, W. M. Chen, H. P. Xin, Y. G. Hong, and C. W. Tu, Phys. Rev. B **70**, 085209 (2004).
[10] B. Fluegel, Y. Zhang, J. F. Geisz, and A. Mascarenhas, Phys. Rev. B **72**, 073203 (2005).
[11] S. V. Dudiy, A. Zunger, M. Felici, A. Polimeni, M. Capizzi, H. P. Xin, and C. W. Tu, Phys. Rev. B **74**, 155303 (2006).
[12] M. Gungerich, P. J. Klar, W. Heimbrodt, G. Weiser, J. F. Geisz, C. Harris, A. Lindsay, and E. P. O'Reilly, Phys. Rev. B **74**, 241202(R) (2006).
[13] B. Gil, M. Baj, J. Camassel, H. Mathieu, C. Benoit a la Guillaume, N. Mestres, and J. Pascual, Phys. Rev. B **29**, 3398 (1984).
[14] M. I. Eremets, O. A. Krasnovskij, V. V. Struzhkin, and A. M. Shirokov, Semicond. Sci. Technol. **4**, 267 (1989).
[15] B. Gil and M. Leroux, Phys. Status Solidi A **195**, 485 (2003).
[16] J. L. Merz, A. Baldereschi, and A. M. Sergent, Phys. Rev. B **6**, 3082 (1972).

[17]H. Mathieu, L. Bayo, J. Camassel, and P. Merle, Phys. Rev. B **22**, 4834 (1980).
[18]B. Gil, J. Camassel, J. P. Albert, and H. Mathieu, Phys. Rev. B **33**, 2690 (1986).
[19]B. Gil and H. Mariette, Phys. Rev. B **35**, 7999 (1987).
[20]M. D. Sturge, A. T. Vink, and F. P. J. Kuijpers, Appl. Phys. Lett. **32**, 49 (1978).
[21]M. D. McCluskey, Y. M. Gupta, C. G. Van de Walle, D. P. Bour, M. Kneissl, and N. M. Johnson, Appl. Phys. Lett. **80**, 1912 (2002).
[22]S. J. Turneaure and Y. M. Gupta, Appl. Phys. Lett. **91**, 201913 (2007).
[23]P. Grivickas, M. D. McCluskey, and Y. M. Gupta, Phys. Rev. B **75**, 235207 (2007).
[24]P. Grivickas, M. D. McCluskey, and Y. M. Gupta, Appl. Phys. Lett. **92**, 142104 (2008).
[25]J. F. Geisz, R. C. Reedy, B. M. Keyes, and W. K. Metzger, J. Cryst. Growth **259**, 223 (2003).
[26]Y. M. Gupta, *COPS code* (SRI International, Menlo Park, CA, 1976).
[27]S. C. Jones, M. C. Robinson, and Y. M. Gupta, J. Appl. Phys. **93**, 1023 (2003).
[28]S. C. Jones and Y. M. Gupta, J. Appl. Phys. **88**, 5671 (2000).
[29]L. M. Barker and R. E. Hollenbach, J. Appl. Phys. **41**, 4208 (1970).
[30]A. Polian and M. Grimsditch, Phys. Rev. B **60**, 1468 (1999).
[31]X. A. Shen and Y. M. Gupta, Phys. Rev. B **48**, 2929 (1993).
[32]J.-K. Hyun, S. M. Sharma, and Y. M. Gupta, J. Appl. Phys. **84**, 1947 (1998).
[33]P. J. Dean, Phys. Rev. **157**, 655 (1967).
[34]D. R. Wight, J. Phys. C **1**, 1759 (1968).
[35]Y. Zhang and W. Ge, J. Lumin. **85**, 247 (2000).
[36]B. Gil, J. Camassel, P. Merle, and H. Mathieu, Phys. Rev. B **25**, 3987 (1982).
[37]H. Mathieu, P. Merle, E. L. Ameziane, B. Archilla, and J. Camassel, Phys. Rev. B **19**, 2209 (1979).